Phase-Separated, Epitaxial, Nanostructured $LaMnO_3$+MgO Composite Cap Layer Films for Propagation of Pinning Defects in $YBa_2Cu_3O_{7-\delta}$ Coated Conductors

Sung Hun Wee[1,2], Junsoo Shin[1], Claudia Cantoni[1], Harry M. Meyer[1], Sy Cook[1], Yuri L. Zuev[1], Eliot Specht[1], Xuming Xiong[3], M. Parans Paranthaman[1], V. Selvamanikcam[3], and Amit Goyal[1]

[1] *Oak Ridge National Laboratory, Oak Ridge, TN 37831, U.S.A.*
[2] *Department of Materials Science and Engineering, University of Tennessee, Knoxville, TN 37996, U.S.A.*
[3] *University of Houston, Mechanical Engineering Department, Houston, TX 77204-4006, U.S.A.*

Received March 19, 2009; accepted May 7, 2009; published online June 12, 2009

Nanostructural modulation in the cap layer used in coated conductors can be a potential source for nucleating microstructural defects into the superconducting layer for improving the flux-pinning. We report on the successful fabrication of phase separated, epitaxial, nanostructured films comprised of $LaMnO_3$ (LMO) and MgO via pulsed laser deposition (PLD) on biaxially-textured MgO metallic templates with a LMO buffer layer. Scanning Auger compositional mapping and transmission electron microscopy cross sectional images confirm the nanoscale, spatial modulation corresponding to the nanostructured phase separation in the film. $YBa_2Cu_3O_{7-\delta}$ films (0.8 μm thick) grown using PLD on such phase separated, nanostructured cap layers show reduced field dependence of the critical current density with an α value of ~0.38 (in $J_c \sim H^{-\alpha}$). © 2009 The Japan Society of Applied Physics

DOI: 10.1143/APEX.2.063008

Second generation (2G), high temperature superconducting (HTS) wires or coated conductors are expected to be used for a wide range of large-scale, electric power applications such as underground transmission cables, transformers, motors, generators, etc.[1] 2G HTS wires have a complex composite, multilayered architecture typically comprised of epitaxial $REBa_2Cu_3O_{7-\delta}$ (RE = rare earth elements, REBCO) films on textured metallic templates with multiple oxide buffer layers.[1] In such multilayered architectures, buffer layers are needed to prevent interdiffusion of elements between the metal alloy substrate and REBCO, to reduce lattice mismatch between REBCO and the metal substrate, and to improve overall crystallographic texture in the REBCO layer. Typically these functions are met by use of multiple buffer layers. It is desirable to combine several of these functions into one layer or to create multifunctional buffer layers which besides performing one of these stated functions, also provides an additional beneficial use.

For most applications, HTS wires are required to sustain a high critical current density, J_c, in the presence of high applied magnetic fields. The in-field superconducting performance of the HTS wires depends critically on the ability of non-superconducting defects within the REBCO film to immobilize or pin magnetic flux lines (or vortices), the motion of which produces undesirable dissipation. Hence, it is necessary to optimize the density, size and geometry of nanoscale defects within REBCO films to maximize their pinning potential and consequently, the in-field J_c. Several approaches to control such nanoscale, non-superconducting defects have been reported.[2–13] For example, it has been shown that incorporation of a three dimensional (3D) self-assembled structure of $BaZrO_3$, YSZ and $BaSnO_3$ nanodots into REBCO films is a very effective approach to enhance the pinning, particularly for $H \parallel c$.[5–12]

In this paper, we report on the use of a phase-separated, epitaxial, nanocomposite film as a multifunctional buffer layer that not only performs the function of a cap layer but also results in reduced field dependence of J_c in epitaxial $YBa_2Cu_3O_{7-\delta}$ (YBCO) films grown on this layer. The specific material combination of the phase separated film reported in this paper corresponds to a $LaMnO_3$ (LMO)+MgO nanostructured, composite film. Such phase-separated, epitaxial nanostructures in the phase-separated LMO+MgO composite cap layer can potentially provide a route to the reproducible generation of additional defects and/or strains within superconducting films.

LMO+MgO composite films with 25 vol % MgO additions were prepared using pulsed laser ablation (PLD) on short segments ($0.5 \times 2\,cm^2$) of standard ion-beam-assisted deposition (IBAD) MgO templates with a LMO layer obtained from SuperPower. Subsequently, YBCO films, 0.8 μm in thickness were grown on the top of the LMO+MgO composite layer using PLD (10 Hz, $2\,J/cm^2$) at 790 °C in 230 mTorr of O_2 LMO+MgO nanostructured, phase separated films (~65 nm thick) were deposited using PLD (5–10 Hz, $2\,J/cm^2$) at 850 °C in 100 mTorr of O_2. After deposition, samples were *in-situ* annealed at $T_s = 500\,°C$ and $P(O_2) = 500$ Torr. Ag electrodes were then sputtered onto the films followed by *ex-situ* annealing at 450 °C for 1 h in flowing O_2 gas. Transport properties of the samples were measured using the standard four-point probe method. The nanoscale, compositional modulation in the phase-separated film was analyzed using scanning Auger spectroscopy. Cross sectional microstructures were characterized by TEM. Texture and phase analysis was done using X-ray diffraction.

An X-ray diffraction, θ–2θ scan for a LMO+MgO composite film grown on a LMO/IBAD-MgO/Hastelloy substrate is shown in Fig. 1. Also included in the figure for comparison is the θ–2θ scan for standard LMO/IBAD-MgO/Hastelloy template without the LMO+MgO layer (using identical conditions with same sample dimension, X-ray power and scan rate). Both samples with and without the LMO+MgO layer show only strong LMO(h00) and MgO(200) peaks with small substrate peaks from the Hastelloy substrate. The LMO and MgO peaks are significantly intensified by growth of the LMO+MgO layer on the LMO/IBAD-MgO/Hastelloy template. The in- and out-of-plane texture, determined by estimating the full-width-half-maximum (FWHM) values of ω and φ scans for LMO and MgO reflections, were also improved by the growth of the LMO+MgO layer, indicating excellent cube-on-cube epitaxy for the LMO+MgO composite layer.

Figure 2 shows an Auger compositional map generated

 © 2009 The Japan Society of Applied Physics

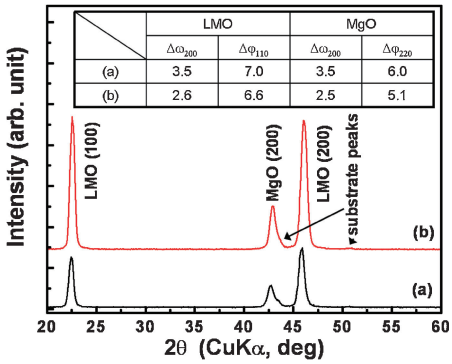

	LMO		MgO	
	$\Delta\omega_{200}$	$\Delta\varphi_{110}$	$\Delta\omega_{200}$	$\Delta\varphi_{220}$
(a)	3.5	7.0	3.5	6.0
(b)	2.6	6.6	2.5	5.1

Fig. 1. The θ–2θ scans for (a) IBAD-MgO template with LMO buffer layer (b) LMO+MgO composite film grown on IBAD-MgO template with LMO buffer layer.

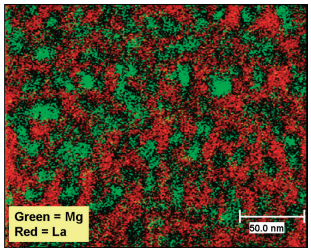

Fig. 2. Compositional mapping using Auger spectroscopy for LMO+25 vol % MgO nanocomposite films. Green and red colors stand for Mg and La elements, respectively.

from the surface of the LMO+25 vol % MgO film. Green and red colors indicate Mg and La elements, respectively. The presence of distinctive green and red colored regions indicates separation of MgO and LMO phases at the nanoscale. Nanometer-sized MgO islands surrounded by LMO matrix can be observed.

A more detailed examination of phase separation in the LMO+MgO layer was performed using TEM on a cross-section sample prepared using the FIB technique. Figure 3(a) contains a low magnification TEM image showing the entire cross section of LMO+MgO composite film. The thickness of LMO+MgO film is estimated to be ~65 nm. The upper white dashed line in Figs. 3(a) and 3(b) outlines the interface between the crystalline composite film and the amorphous Pt protective layer deposited prior to TEM sample preparation. The sharp interface between the LMO film and the composite LMO+MgO film is also indicated. In the LMO+MgO layer, moiré fringes are observed where the MgO and LMO lattices overlap within the thickness of the TEM foil. Many nanocolumnar shaped as well as shorter or rounder MgO particles can be seen, as indicated by the dashed ovals. Figure 3(b) shows a low magnification, scanning transmission electron microscope (STEM) *Z*-contrast image of the LMO+MgO layer. Dark and bright contrast corresponds to the MgO and LMO phases respectively. The elongated dark-contrast regions highlighted using dashed white lines indicate individual MgO nanocolumns. It is also interesting to note that some of these MgO columns extend beyond the film surface as indicated by arrows in Figs. 3(a)–3(b). Figure 3(c) is a higher magnification TEM image showing one such MgO nanocolumn protruding out from the film. The MgO nanocolumn has a diameter of ~10 nm and extrudes more than 10 nm above the film surface.

Superconducting properties of YBCO grown on standard LMO/IBAD-MgO/Hastelloy templates with and without the LMO+MgO phase-separated, nanocomposite cap layer are shown in Fig. 4, where the field and angular dependence is illustrated for $J_c/J_c(\mathrm{sf})$, normalized J_c with respect to J_c at self field, 77 K. Both samples were measured to have similar superconducting transition temperature, T_c, of 87.5–87.7 K. A YBCO film grown on the template with the LMO+MgO layer was measured to have a transport J_c of 1.3 MA/cm^2 at 77 K, self-field. This J_c value is smaller than the highest J_c (2.8 MA/cm^2) we have obtained previously for YBCO films

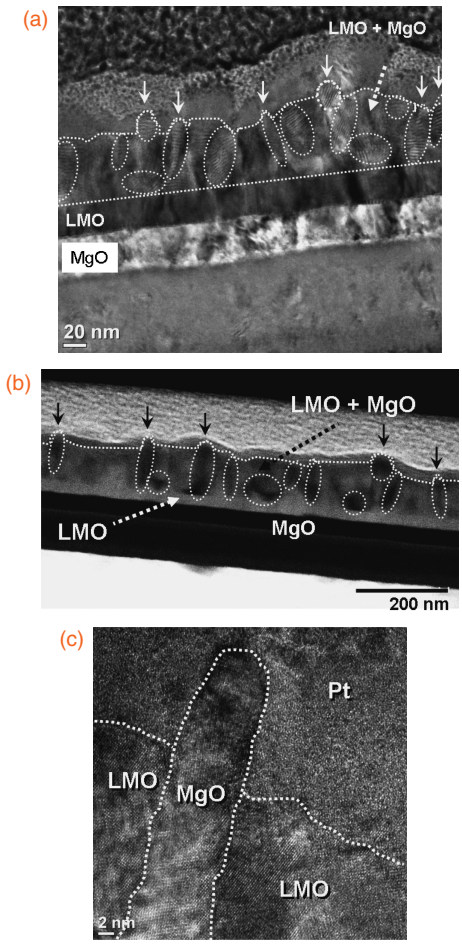

Fig. 3. Cross sectional TEM image for the phase separated LMO+25 vol % MgO composite film. (a) Bright field and (b) scanning *Z*-contrast images for the entire cross-section of the epitaxial, phase separated, layer on LMO buffered, IBAD-MgO, metallic template. In (a), moiré fringes highlight the MgO phase. In (b), Bright and dark contrast correspond to LMO and MgO phases, respectively. (c) High resolution cross section image showing a MgO nanocolumn that grew above the film surface.

of the same thickness grown on the standard LMO/IBAD-MgO/Hastelloy templates of similar quality. The lower self-field J_c could be attributed to the existence of *a*-axis oriented particles in the YBCO film, which is not observed in YBCO films grown on standard IBAD-MgO substrates, as confirmed by X-ray diffraction result shown in Fig. 5. Volume % of *a*-axis particles estimated by (102) χ-scan is ~6.6%. Formation of *a*-axis growth in the film should be caused by the poor surface condition of the LMO+MgO composite

© 2009 The Japan Society of Applied Physics

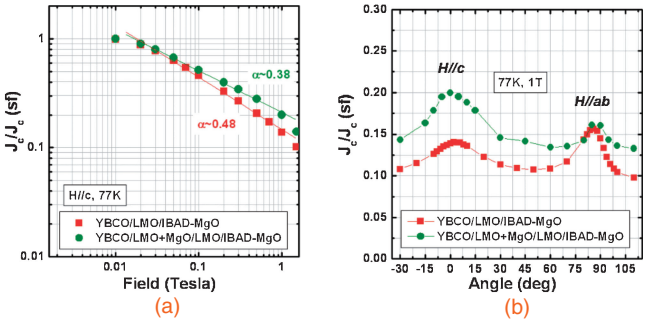

Fig. 4. (a) Field dependence of J_c/J_c(sf), at 77 K for 0.8-μm-thick YBCO films grown on LMO (sputtered)/IBAD-MgO/Hastelloy metallic template with and without the PLD grown LMO+MgO composite layer. (b) Angular dependence of J_c/J_c(sf) at 77 K, 1 T from −30 to 115° with respect to $H \parallel c$ for the films in (a).

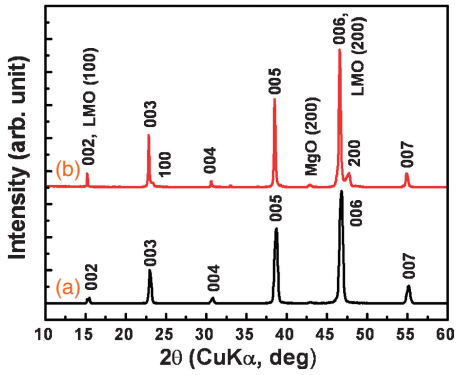

Fig. 5. The θ–2θ scans for (a) 0.8-μm-thick YBCO film grown on standard IBAD-MgO template and (b) the YBCO film grown on the template with LMO+MgO composite layer.

layer. AFM results confirmed that the LMO+MgO layer has a very rough surface with an rms roughness of ∼15 nm (the roughness of the LMO layer on which the composite layer was grown has a roughness of ∼1 nm). Further work is ongoing to improve the self-field J_c of YBCO films by removing *a*-axis growth and improving the surface morphology or roughness of the LMO+MgO composite cap layer. Nevertheless, in the presence of applied magnetic fields, a reduced fall-off of J_c with field is observed for YBCO films grown on the nanocomposite film. The YBCO film grown on the LMO+MgO layer exhibits a lesser reduction of J_c and a reduced α value of ∼0.38 in $J_c \sim H^{-\alpha}$ [Fig. 4(a)]. In addition, the angular dependence of J_c/J_c(sf) at 77 K, 1 T reported in Fig. 4(b) also shows a much stronger peak for $H \parallel c$, indicating improved *c*-axis correlated pinning. It was reported that the pinning is enhanced by linear defects stemming from surface-decorated nanoscale particles on the substrate.[4,14] The enhancement mechanism in the pinning in this study seems to be similar, but this approach offers the possibility to control the density and size of nanoparticles/nanorods to propagate linear defects into the YBCO film without an additional processing step (if this layer is adopted as the cap layer). It is recognized that the self-field J_c needs to be improved to the level of the highest J_c demonstrated previously for YBCO films of the similar thickness grown by *any* technique on LMO buffered, IBAD-MgO metallic templates with the same texture. Work is ongoing to address this goal by experimenting with PLD deposition conditions (It is likely that optimal PLD depositions are different for the growth of YBCO films on PLD deposited LMO layers) as well as by developing the optimum buffer deposition conditions which reduces the surface roughness of the phase separated layer. We are also experimenting with the processing conditions of the phase separated layer to enable control of both the size and density of the MgO nanoparticles in the phase separated LMO+MgO film.

In summary, a phase separated, nanostructured, epitaxial, cap layer comprised of LMO+25 vol % MgO was epitaxially grown on standard LMO buffered, IBAD-MgO metallic templates. Compositional modulation generated by the nanoscale phase separation was clearly observed using Auger spectroscopy and cross sectional TEM. Epitaxial PLD-YBCO films grown on such a nanoscale, phase separated, LMO+MgO cap layer exhibited reduced field dependence of J_c with a α value of ∼0.38 (in $J_c \sim H^{-\alpha}$) and a pronounced peak in the angular dependence of J_c for $H \parallel c$.

Acknowledgments Y. L. Zuev would like to thank Oak Ridge Associated Universities for a postdoctoral fellowship. We would like to thank Cliffard C. Davisson for preparing the LMO+MgO target by powder mixing, compaction and sintering. A. Goyal would like to thank SuperPower Inc. for providing the Hastelloy substrates with the multilayer configuration of IBAD MgO layer/homoepitaxial MgO layer/epitaxial $LaMnO_3$. Research was sponsored by the US Department of Energy, Office of Electricity Delivery and Energy Reliability-Superconductivity Program, under contract DE-AC05-00OR22725 with UT-Battelle, LLC managing contractor for Oak Ridge National Laboratory.

1) *Second Generation HTS Conductors*, ed. A. Goyal (Kluwer, Boston, MA, 2005).
2) T. Haugen, P. N. Barnes, R. Wheeler, F. Meisenkothen, and M. Sumption: Nature **430** (2004) 867.
3) K. Matsumoto, T. Horide, A. Ichinose, S. Horii, Y. Yoshida, and M. Mukaida: Jpn. J. Appl. Phys. **44** (2005) L246.
4) T. Aytug, M. Paranthaman, A. A. Gapud, S. Kang, H. M. Christen, K. J. Leonard, P. M. Martin, J. R. Thompson, D. K. Christen, R. Meng, I. Rusakova, C. W. Chu, and T. H. Johansen: J. Appl. Phys. **98** (2005) 114309.
5) A. Goyal, S. Sathyamurthy, and T. Atyug: paper presented at the 2004 Annual Peer Review for the U.S. Superconductivity Program for Electric Systems, July 27–29, 2004, Washington, D.C. [http://www.energetics.com/meetings/supercon04/pdfs/presentations/f_rabits_strategic_talk_ffy04_final.pdf].
6) A. Goyal, S. Kang, K. J. Leonard, P. M. Martin, A. A. Gapud, M. Varela, M. Paranthaman, A. O. Ijaduola, E. D. Specht, J. R. Thomson, D. K. Christen, S. J. Pennycook, and F. A. List: Supercond. Sci. Technol. **18** (2005) 1533.
7) S. H. Wee, A. Goyal, P. M. Martin, M. Paranthaman, and L. Heatherly: Supercond. Sci. Technol. **19** (2006) L42.
8) S. Kang, A. Goyal, J. Li, A. A. Gapud, P. M. Martin, L. Heatherly, J. R. Thompson, D. K. Christen, F. A. List, M. Paranthaman, and D. F. Lee: Science **311** (2006) 1911.
9) S. H. Wee, A. Goyal, Y. L. Zuev, S. Cook, and L. Heatherly: Supercond. Sci. Technol. **20** (2007) 789.
10) S. H. Wee, A. Goyal, J. Li, Y. L. Zuev, and S. Cook: J. Appl. Phys. **102** (2007) 063906.
11) P. Mele, K. Matsumoto, T. Horide, A. Ichinose, M. Mukaida, Y. Yoshida, S. Horii, and R. Kita: Supercond. Sci. Technol. **21** (2008) 032002.
12) S. H. Wee, A. Goyal, Y. L. Zuev, and C. Cantoni: Supercond. Sci. Technol. **21** (2008) 092001.
13) S. H. Wee, A. Goyal, Y. L. Zuev, and C. Cantoni: Appl. Phys. Express **1** (2008) 111702.
14) K. Matsumoto, T. Horide, A. Ichinose, S. Horii, Y. Yoshida, and M. Mukaida: Jpn. J. Appl. Phys. **44** (2005) L246.

© 2009 The Japan Society of Applied Physics